Exploring the Internal Radiative Efficiency of Selective Area Nanowires

Cavalli, A; Haverkort, JEM; Bakkers, Erik

DOI
10.1155/2019/6924163

Publication date
2019

Document Version
Final published version

Published in
Journal of Nanomaterials

Hindawi
Journal of Nanomaterials
Volume 2019, Article ID 6924163, 13 pages
https://doi.org/10.1155/2019/6924163

Research Article

Exploring the Internal Radiative Efficiency of Selective Area Nanowires

A. Cavalli[1], **J. E. M. Haverkort**[1] **and E. P. A. M. Bakkers**[1,2]

[1]*Department of Applied Physics, Eindhoven University of Technology, Netherlands*
[2]*Kavli Institute of Nanoscience, Delft University of Technology, Netherlands*

Correspondence should be addressed to A. Cavalli; a.cavalli.phd@gmail.com

Received 16 November 2018; Revised 6 February 2019; Accepted 12 February 2019; Published 2 June 2019

Academic Editor: Yasuhiko Hayashi

Nanowires are ideal building blocks for next-generation solar cell applications. Nanowires grown with the selective area (SA) approach, in particular, have demonstrated very high material quality, thanks to high growth temperature, defect-free crystalline structure, and absence of external catalysts, especially in the InP material system. A comprehensive study on the influence of growth conditions and device processing on optical emission is still necessary though. This article presents an investigation of the nanowire optical properties, performed in order to optimize the internal radiative efficiency. In an initial preamble, the motivation for this study is discussed, as well as the morphology and crystallinity of the nanowires. The effect on the nanowire photoluminescence of several intrinsic and extrinsic parameters and factors are then presented in three sections: first, the influence of basic growth conditions such as the temperature and the precursor ratio is studied. Subsequently, the effects of varying dopant molar flows are explored, keeping in mind the intended solar cell application. Third, the manner in which the processing and the passivation affect the nanowire optical emission is discussed. Precise control of the growth conditions allows maximizing the nanowire internal radiative efficiency and thus their performance in solar cells and other optoelectronic devices.

1. Introduction

Photovoltaic (PV) technology can provide a substantial portion of electricity generation, and great progress has been observed in the recent decades, with the field projected to have 1 TW of installed power by 2020. Its development is still curbed by the opposite thrusts of low cost and high efficiency though. Solar cells based on nanowire arrays hold promise to solve the current impasse, as they have many advantages: they allow fast growth [1] and lower material consumption by enabling substrate reuse [2] and thanks to high absorption-to-volume ratio through light-trapping [3, 4]. Furthermore, their tolerance to lattice mismatch allows unprecedented material integration [5], and their geometry allows unconventional current extraction designs [6, 7]. Finally, they have an enhanced performance compared to planar layers, as a result of geometry-related increased photon outcoupling and reduced bulk recombination due to their lower volume [8]. Most nanowire growth is carried out by using the vapor-liquid-solid method, which uses a catalyst particle to grow a pillar-shaped structure [9–11]. Selective area nanowires, instead, are obtained by using a substrate covered with a growth mask, from which nanostructures shaped as columns can be grown by carefully tuning the reactor conditions. They have been extensively studied in the last 10 years, with extremely promising results in lasing, transistor, and solar cell applications [12–14]. In particular, selective area InP nanowires have demonstrated very good PV device performance when measured in a single nanowire geometry [15, 16].

The performance can be further improved by careful examination of growth conditions and device processing, and their influence on the photoluminescence emitted by the nanowires. By optimizing the optical emission, the open-circuit voltage can be substantially enhanced [8]. The external radiative efficiency $\eta_{\mathrm{ext}}^{\mathrm{PL}}$ is in fact expressed as the ratio between the number of radiative recombination events that lead to photons emitted out of the device and the total

recombination events. The η_{ext}^{PL} is closely related to the efficiency of a solar cell device, in particular to the open-circuit voltage V_{oc}, as expressed clearly by the equation

$$V_{oc} = V_{oc}^{rad} - \frac{k_B T}{q} \left| \ln \left(\eta_{ext}^{PL} \right) \right|, \quad (1)$$

where V_{oc}^{rad} represents the V_{oc} in the radiative limit, meaning with external radiative efficiency of 1; k_B is Boltzmann's constant; T is the device temperature; and q is the electronic charge. This equation can be rewritten in terms of the PL intensity of the sample, which, being directly proportional to the η_{ext}^{PL}, becomes a direct relation between the PL and the V_{oc}:

$$I_{PL}(E) = a(E) I_{bb}(E) \left(\exp \left(\frac{qV_{oc}}{kT} \right) - 1 \right), \quad (2)$$

where E is the energy of the emission, kT is the thermal energy (25.7 meV at room temperature), $a(E)$ is the absorptivity, and $I_{bb}(E)$ is the blackbody emission intensity. An increase in the radiative efficiency is then directly connected to an increase in the PL intensity, which thus corresponds to a V_{oc} enhancement.

Additionally, if the internal radiative efficiency η_{int}^{PL} is low (<0.1) as in the case of the nanowires considered here, the η_{ext}^{PL} can be defined as

$$\eta_{ext}^{PL} = \eta_{int}^{PL} \times \bar{P}_{esc}, \quad (3)$$

where $\bar{P}_{esc}$ is the average photon escape probability.

In this article, the focus is on the maximization of the first term by changing the growth conditions and studying the influence of device processing, assuming all along that the second factor is constant.

2. Methods

A 50 nm thick silicon nitride layer is used as the growth mask, patterned by soft contact nanoimprint lithography [17] on a (111)A-oriented p-doped InP substrate (Zn doping carrier concentration 2×10^{18} cm^{-3} from AXT, USA). InP nanowires are normally obtained at relatively high temperature (650–750°C) and low ratio between group V (PH_3 for P) and group III (TMI for In) precursors (10 – 200), at a pressure of 100 mbar in an H_2 flow of 15 l/min, in a laminar MOVPE reactor. Diethylzinc (DEZn) is used as the p-dopant, with molar fractions typically between 1×10^{-6} and 7.4×10^{-5}. Di-tert-butyl silane (DTBSi) is used as n-dopant, with molar fractions within 5×10^{-9} and 1.6×10^{-6}. The nanowire arrays are imaged on cleaved samples by using a Zeiss Sigma field emission scanning electron microscope (SEM) operating at 3 kV. Imaging is performed at either 30° or 90° tilt compared to the normal to the surface. TEM and STEM analyses were conducted using a JEOL JEM-ARM200F aberration-corrected TEM operated at 200 kV, while for the chemical analysis, energy-dispersive X-ray (EDX) measurements were carried out using a 100 mm^2 Centurio silicon drift detector (SDD).

After growth, either the photoluminescence (PL) of nanowires is measured directly or nanowire array solar cell devices are fabricated using a process described previously [18, 19]. A custom-built PL setup is used to measure the optical emission of the nanowires. Microphotoluminescence (μPL) studies are carried out on nanowire arrays (either as-grown or processed). To image the specimen and to focus the laser beam, lenses or objectives (with 50x/100x magnification) are used. Nanowire samples are mounted on the cold finger of a flow cryostat, which allows controlling the temperature between helium cooled (~4 K) and room temperature (293 K). All measurements in this article are performed at 300 K. The cryostat is mounted on an $x - y$ translation stage for basic positioning, while fine aligning in x, y, and z directions is performed by piezoelectric actuators (with 30 nm resolution) controlling the objective. The optical emission of the NW is directed towards the entrance slit of a triple grating SP2500A (Princeton Instruments, 50 cm focal length). A white lamp coupled with a camera is used for controlling the location of the incident laser on the sample. Time-resolved PL measurements are done using a time-correlated single-photon counting module (TCSPC, PicoHarp 300), which measures the time delay between the sample excitation and the arrival of emitted photons at a single photon detector (SPD). After the measurement is repeated many times, the delay times are sorted in a histogram plotting the time distribution of the emission after the excitation pulse [20]. As the temperature has an effect on the PL, all measurements are performed at room temperature (~300 K), which is the solar cell operating temperature.

3. Results and Discussion

3.1. Selective Area Nanowire Morphology and Crystallinity. In Figures 1(a) and 1(b) are presented two typical SEM images of undoped selective area nanowires, grown at 730°C for 20 min at a V/III ratio of 114 and TMI molar fraction of 4.7×10^{-5}. The morphology of the sample is extremely uniform, as all nanowires have a hexagonal cross section and have very homogeneous length and diameter. In Figures 1(c)–1(f), several TEM-acquired images are shown, displaying the crystalline properties of a nanowire with a $p^+ - p - i - n - n^+$ doping profile as depicted in panel (c). The doping transitions in the growth procedure are sharp, with doping molar fractions $7.4 \times 10^{-5} - 10^{-6} - 0 - 4 \times 10^{-7} - 1.6 \times 10^{-6}$, respectively. Apart from the very highly n-doped top part of the nanowire, which has a high density of stacking faults, the nanowires have a perfect wurtzite crystalline structure, showing no effect of doping on the crystallinity. Undoped nanowires have an identical crystalline structure. A sample grown with linearly increasing n-doping during growth, characterized by both atom probe tomography and TEM [21], reveals no stacking faults up to a doping molar flow of ~10^{-6}, further proving the purity of the crystalline structure.

The growth of nanowires with a wurtzite crystalline structure on a zinc blende substrate is explained by the fact

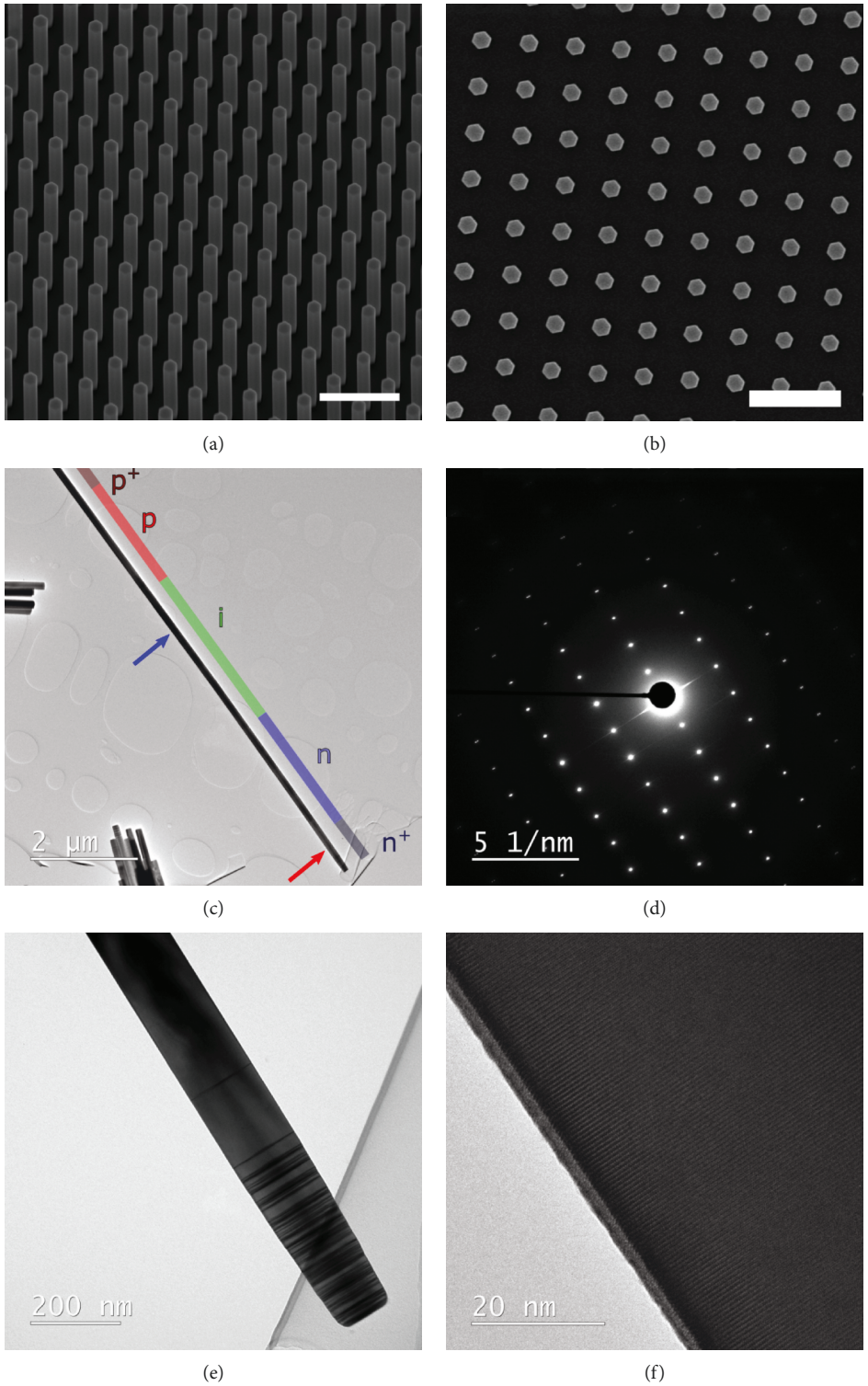

Figure 1: SEM and TEM of selective area InP nanowires. (a) SEM image, inclined 30° respective to the normal, of SA i – InP. The scale bar is 1 μm. (b) Top view SEM image of i – InP nanowires taken normal to the substrate. The scale bar is 1 μm. (c) Overview of a bright-field TEM image of a representative nanowire with a $p^+ - p - i - n - n^+$ doping profile. The nominal design of the doping profile is depicted in the image as well. (d) Selected area electron diffraction pattern, acquired from a 1.3 μm-long segment of the middle part of the nanowire, displaying the wurtzite structure. (e) BF-TEM image of the top of the wire (red arrow panel (c)), displaying the defected top n^--doped part and the defect-free rest of the NW. (f) HRTEM image of the center of the nanowire (blue arrow panel (c)), displaying the perfect wurtzite structure.

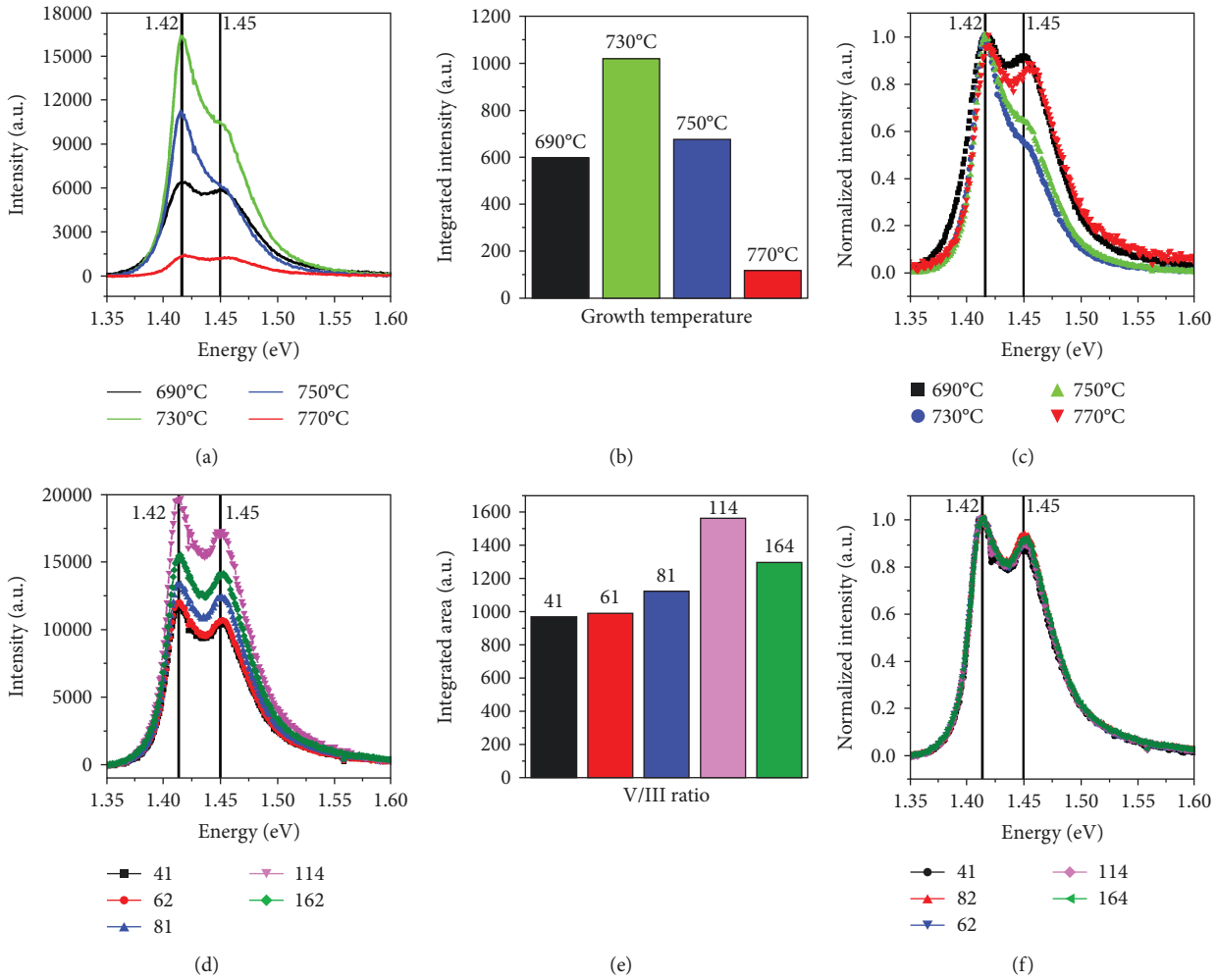

Figure 2: Effect of the growth temperature and V/III ratio on PL intensity. (a) Series of spectra of the absolute PL intensity versus energy, measured for samples grown at different temperatures between 690°C and 770°C, with a V/III ratio of 114. The intensity increases when the temperature is raised up to 730°C, but decreases strongly at higher temperatures. Two vertical lines, at 1.42 eV and 1.45 eV, indicate the position of the *A* and *B* transitions. (b) Peak integrated PL intensity, as a function of growth temperature, measured at a laser power equivalent to 10 suns, showing the same trend as in panel (a). (c) Series of spectra normalized to the maximum of each one, measured on samples grown at different temperatures. (d) Series of spectra of the absolute PL intensity versus energy, measured for samples grown at different V/III ratios, between 41 and 164, at a growth temperature of 730°C. The intensity increases when V/III is raised up to 114, but decreases strongly at a higher ratio. Two vertical lines, at 1.42 eV and 1.45 eV, indicate the position of the *A* and *B* transitions. (e) Peak integrated PL intensity, as a function of V/III ratio, measured at a laser power equivalent to 10 suns, showing the same trend as in panel (d). (f) Normalized spectra calculated from the absolute spectra of panel (d), highlighting the negligible difference between the spectra.

that in the typical SA growth conditions (high temperature and low V/III ratio), the desorption of P is significant, and thus the surface is terminated with In atoms. In this configuration, growth along the 111*A* is only possible if additional In atoms are adsorbed: the WZ stacking though is favored as the ABAB stacking is more energetically stable, due to the larger Coulomb interaction between In atoms and the second nearest pair of In and P [22].

3.2. $\eta_{\text{int}}^{\text{PL}}$*: Effect of Growth Temperature and* V/III *Ratio.* The first two parameters taken into account are basic growth settings such as the temperature in the reactor and the V/III ratio, which are the two most elementary variables adjustable during MOVPE growth.

Temperature is a crucial parameter in nanowire growth, as it has been shown to change the crystalline structure of the nanowires, to influence the concentration of intrinsic and extrinsic defects, and in general to dramatically affect optoelectronic properties of nanowires [23–25]. In particular, for InP selective area growth, temperature increase beyond ~675°C is demonstrated to lead to pure wurtzite crystalline structure and a strong enhancement of PL intensity [12]. In Figure 2(a), a series of PL spectra, acquired at room temperature for samples grown at increasing temperatures, up to 770°C, is depicted. No growth is observed at temperatures of 780°C or higher. In all cases, irrespective of the incident laser power, the PL spectra show a peak with a shoulder at higher energy, representing, respectively, the band edge

emission and the split-off valence band (often labeled as A and B transitions) of WZ InP nanowires. The ratio between the two peak intensities is different among different samples, hinting at a complex underlying mechanism. While all measurements are performed as-grown, with nanowires standing on the (111)A InP substrate, no contribution to the PL from the bulk ZB InP, expected at an energy of 1.35 eV, is observed. The intensity, and thus the optical quality expressed as $\eta_{\text{ext}}^{\text{PL}}$, increases for higher growth temperature up to 730°C, while it decreases at higher temperatures. The external radiative efficiency for the best sample, which is also one of the highest among all the samples following in this article (since both doping and processing decrease the PL performance), is estimated as ~10^{-4} at 1 – sun illumination intensity. This value is comparable to what has been measured for InP bulk layers grown by MOCVD, but lower than nanowires etched by ICP-RIE (respectively, 5.2×10^{-5} and 7×10^{-4}) [26]. The second parameter to be investigated is the V/III ratio: a series of samples is realized by keeping the TMI molar fraction constant at 4.7×10^{-5}, and varying the PH_3, such that the proportion between the two is adjusted between 41 and 164. A clear increase is witnessed up to a quotient of 114, while a further raise is detrimental (Figures 2(d)–2(e)). No influence of the V/III ratio on the shape of the PL peaks is observed in this case (Figure 2(f)).

The PL intensity in this case is influenced mainly by a modification in the density of point defects, such as the introduction of P vacancies [27], which are included because of the increased evaporation of precursors and change in the surface reconstruction of the nanowire top surface, which are both expected with rising temperature [28]. Radiative recombination is then reduced at extremely high temperature by the accumulation of point defects. This explanation is supported by the fact that at temperatures higher than 750°C the growth rate is lower, and at 780°C growth stops entirely: as P atoms evaporate progressively more quickly, crystalline growth is not supported anymore, and growth cannot occur. This mechanism also explains the V/III ratio series results, as the high temperature would result in increased precursor evaporation: In from the precursor has high vapor pressure already at lower temperatures, but as the temperature is increased, the phosphorous vapor pressure increases as well. As the group V flow is increased with augmenting V/III ratio though, the density of P-related point defects would be diminished, so that the PL intensity increases. Two other possible explanations that may partially explain the observed effect on PL, in conjunction with the dissociation of P, are the increased precursor pyrolysis at high temperature, which would reduce the incorporation of carbon in the nanowires [29], and an alteration of crystalline structure, as the density of stacking faults has been shown to be dependent on the V/III ratio [12, 30] and to influence the PL intensity [24].

3.3. Doping Effect on $\eta_{\text{int}}^{\text{PL}}$. Control of the presence, the concentration, and the profile of dopant atoms is fundamental for nanowire solar cells: the presence of impurities, charged in respect to their environment, creates the built-in voltage that separates photogenerated carriers and ultimately enables the operation of the device and the power generation. Dopants also influence the PL intensity of the material, which as just discussed impacts profoundly the V_{oc}: careful design of the doping is thus crucial. The PL spectra of doped semiconductors are affected both in shape and in intensity by doping. The Burstein-Moss (BM) shift, an effect also known as Pauli blocking, is caused by the occupation of higher energy states in the conduction band due to the Pauli exclusion rule between carriers. The BM shift hence results in an apparent increase of the bandgap by an amount defined as

$$\Delta E_{\text{BM}} = \frac{\hbar}{2m^*} \left(3\pi^2 n\right)^{2/3}, \tag{4}$$

where $\hbar$ is the reduced Planck constant, while m^* and n are the carrier effective mass and concentration, respectively. As it is dependent on the effective mass, this effect is much more pronounced for electrons than for holes. If generalized for the nonparabolicity of the conduction band, and substituting the values for electrons in bulk ZB InP, the formula then becomes [31]

$$\Delta E_{\text{BM}}(\text{eV}) = 4.73 \times 10^{-14} n_{\text{e}}^{2/3} - 13.83 \times 10^{-28} \times n_e^{4/3}, \tag{5}$$

An effect contrasting the BM shift is the bandgap renormalization (BGR), which leads to a narrowing of the bandgap and an increase in the FWHM. It is caused by many-body effects: the net balance between Coulomb and spin interaction among carriers is attractive, basically resulting in an increase in the valence band edge and a decrease in the conduction band edge. BGR is commonly described by an empirical relation where the coefficients are measured experimentally [31]:

$$\begin{aligned} \Delta E_{\text{BGR}}(\text{eV}) &= \text{An}^{1/3} + Bn^{1/4} + Cn^{1/2} \\ &= 17.2 \times 10^{-9} \times n^{1/3} + 2.62 \times 10^{-7} \times n^{1/4} \\ &\quad + 17.3 \times 10^{-12} \times n^{1/2}. \end{aligned} \tag{6}$$

Since electrons have a rather low effective mass in InP (~0.077), the effective optical gap at room temperature can be easily increased by degenerated doping. While this can be difficult to believe and to achieve for other material systems, it is instead very effective in InP. S doping of 3×10^{19} cm^{-3}, for instance, results in a bandgap of 1.55 eV, an increase by 0.2 eV [32].

In this section, the PL intensity and the minority carrier recombination lifetime are examined for varying p- and n-doping molar flows.

3.3.1. n-Doping. Si is a common dopant element for InP: since it is a group IV material, it is in principle an amphoteric element, as it could function both as a donor and as an acceptor. In practice though, its amphoteric behavior is very limited (only $<10^{-3}$ of all Si atoms behave as an acceptor) [33], so it is used efficiently as a dopant in thin film devices, often employing ditertiarybutyl silane (DTBSi) as a precursor [34, 35]. At growth temperatures above 630°C, Si incorporation in MOCVD growth is efficient and can result in

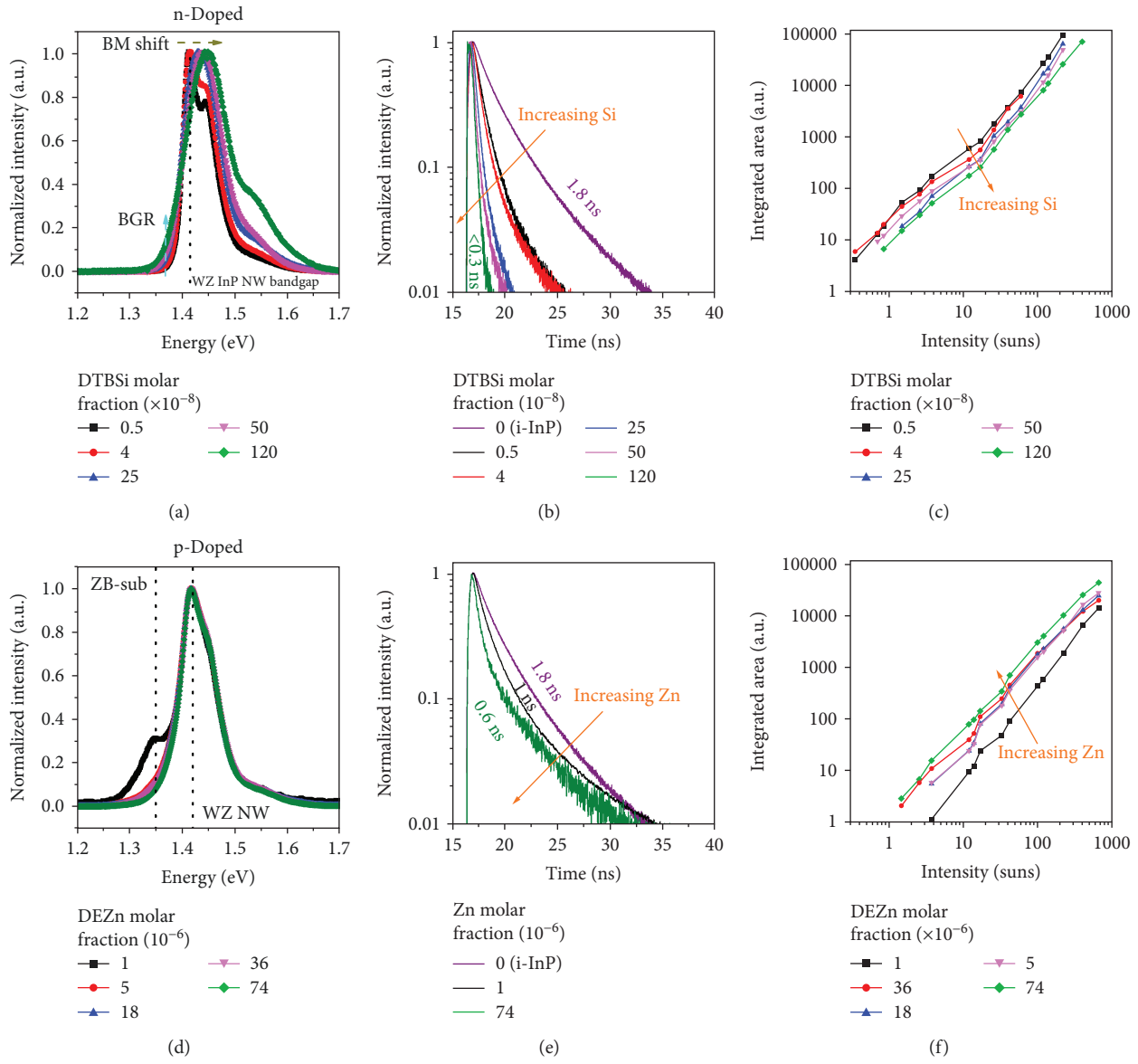

FIGURE 3: Effect of Si and Zn doping on the photoluminescence of nanowires. (a) Series of spectra normalized to the maximum of each one, with different DTBSi-doping molar fractions, between 5×10^{-9} and 1.2×10^{-6}, showing a peak shifting to higher energy and an increase in FWHM, with increasing Si. (b) Time-resolved photoluminescence of the same samples, measured at a laser intensity of 1.4 W/cm^2, highlighting the decreased minority carrier recombination lifetime with larger dopant molar flow. (c) PL intensity as a function of incident laser intensity, converted in multiples of AM1.5 sun intensity: by rising Si incorporation, the emission strength decreases sharply. (d) Series of spectra normalized to the maximum of each one, with different DEZn-doping molar fractions, from 10^{-6} to 7.4×10^{-5}, showing no dependence of the peak shape on the molar flow. (e) Time-resolved photoluminescence of the same samples, measured at a laser intensity of 1.4 W/cm^2, depicting the decrease in minority carrier recombination lifetime corresponding to a larger dopant molar flow. (f) PL intensity as a function of incident laser intensity, converted in multiples of AM1.5 sun intensity: as the DEZn fraction increases, the intensity is monotonically enhanced.

very high concentrations, up to 10^{20} cm^{-3}. Comparable concentrations have been measured by atom probe tomography also in the SA-grown nanowires presented in this article [21], with a linear dependence on the incorporation of the dopant on the molar flow, up to 10^{19} cm^{-3}, without any noticeable influence on the growth rate or the diameter of the nanowires.

A large effect on their optical properties is observed instead, as n-doping is known to influence the shape of the PL spectrum. The combined effect of the BM shift and BGR can be seen in Figure 3(a), where the normalized spectra of as-grown nanowires with several different doping molar fractions (from 5×10^{-9} to 1.2×10^{-6}) are depicted. The PL peak shifts with the increasing doping concentration; at the same time, the FWHM of the peak broadens, as it has been observed also before with increasing the doping concentration [36, 37]. Another peak at ~1.6 eV is evident in most

spectra and is explained by the mixing and superposition of the A and B transitions, due to the larger FWHM associated with a higher doping level. The doping concentration is determined both by the BM and BGR shift and by double-checking this with atom probe tomography (APT) calibration performed on analogous nanowires, grown with a step-like doping distribution from 5×10^{-7} to 9×10^{-6}. At the highest DTBSi molar fraction presented here (1.2×10^{-6}), the doping concentration is thus estimated to be 2×10^{18} cm^{-3}. The dopant concentration appears to be linearly dependent on the molar fraction used, but at low molar fraction values, it is challenging to reliably estimate a concentration value by atom probe measurements. As the combined effect of BM and BGR shifts is very small at concentrations $<5 \times 10^{17}$ cm^{-3}, it is difficult to determine precisely the doping level if the molar fraction is $\lesssim 5 \times 10^{-7}$: a direct proportionality can then only be assumed, as is done later in this article.

Time-resolved PL measurements, performed with a time-correlated single-photon counting (TCSPC) module, presented in Figure 3(b), reveal that increasing the doping concentration impacts dramatically the minority-carrier recombination lifetime: starting from a reference level of 1.8 ns measured for nominally undoped InP nanowires grown in identical conditions, the lifetime decreases sharply with higher DTBSi, until the lifetime is shorter than the instrument response function (limiting the measured laser decay time to ~0.3 ns) at a molar fraction higher than 5×10^{-7}, which corresponds to a doping level of ~10^{18} cm^{-3}, as just discussed.

Regarding the PL intensity, in Figure 3(c), a series of laser power-dependent PL for the different dopants is presented. The laser power is converted to sun intensity, with 1 sun corresponding to the power intensity of AM1.5 illumination (~100 mW/cm^2). It is clear that by increasing the dopant concentration by almost three orders of magnitude, the PL decreases about 6-fold, so that a higher Si molar flow would have a direct negative effect on the V_{OC} which can be extracted from the solar cell, decreasing it by approximately 40 mV. The mechanisms causing this behavior are discussed shortly.

3.3.2. p-Doping. For InP p-type doping, Zn is by far the most common element used: several precursors have been proposed and used, but often diethylzinc is chosen [38]. In the case of p-doping, the Burstein-Moss shift is very small because of the much higher effective mass of holes, which is around one order of magnitude larger than in the case of electrons ($0.6m_0$ compared to $0.08m_0$), reducing heavily its effect. Bandgap renormalization instead has yet again a similar magnitude as the case of Si doping and would give the largest deviation from undoped bandgap. Varying the DEZn molar flow by almost two orders of magnitude (from 10^{-6} to 7.4×10^{-5}) though does not result in any shift, as can be observed in Figure 3(d).

The only difference in the spectra is a result of a variation in the NW PL intensity, which corresponds to a more visible contribution of the zincblende substrate PL (at an energy of 1.35 eV, clearly visible only for the sample grown with 10^{-6} DEZn molar flow). No variation in the peak shape is instead visible, giving thus a first hint that the Zn incorporation in SA nanowires might be inefficient. A clear influence of the doping molar flow can be seen on the minority carrier recombination lifetime of the same samples instead, where the increase in doping concentration results in a shorter lifetime, from around 1 ns (for 10^{-6} fraction) to ~0.6 ns at the highest molar fraction (Figure 3(e)). Furthermore, the PL intensity of p-doped NW has a different trend than for n-doped, as can be seen in Figure 3(f). An increase in PL intensity is observed for increasing doping molar flow, in sharp contrast to the Si-doped case: the intensity is approximately a factor 15 higher for the largest molar fraction, which would result in an enhancement of V_{oc} of ≈70 mV.

3.3.3. p- and n-Doping PL Discussion. For the sake of the subsequent discussion, it is now crucial to distinguish three quantities related to doping. While valid also for the previous sections, they assume particular relevant in this examination:

(1) The dopant molar fraction, expressed as a pure number (without unit), represents simply the nominal ratio between the amount of dopant precursor flowing in the reactor chamber and the total flow present, as can be calculated from the reactor source values (bubbler temperature, partial pressure, and dilution)

(2) The dopant concentration in the semiconductor is expressed as a density (commonly in cm^{-3}) of the number of dopant atoms, or more generally impurity atoms, present in a material. They supply free carriers and can act as radiative or nonradiative recombination centers. Within a certain limit, which roughly speaking corresponds to a dopant concentration much lower than the solubility limit of the element in a material, they are dependent linearly on the molar fraction introduced. The atomic density measured by APT provides a very accurate estimation of this density

(3) The carrier concentration in the semiconductor, also expressed as a density in cm^{-3}, is the number of electrically active (free) carriers diffusing in a semiconductor, or more often in a region of it. The thermally excited carrier density is altered by the presence of dopant atoms and by photogenerated carriers created by incident light. They are influenced by several factors such as temperature, the presence of other impurities, the doping profile design, and bias voltages

As it is clear from the previous two sections, p- and n-doping of SA nanowires have dramatically different behaviors: this is shown further in Figure 4, where the peak energy (scatter dots) as a function of the dopant molar fractions are directly compared.

It appears clear how n-doping strongly influences the position of the peak, effectively leading to a shift in the

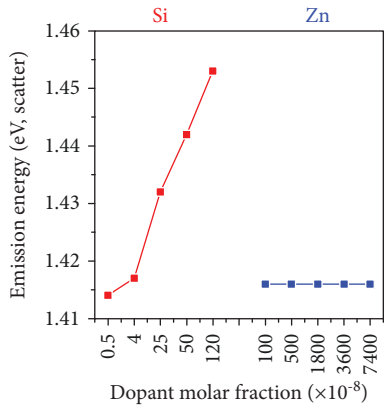

FIGURE 4: Influence of varying n- (in red) and p- (blue) doping molar fraction on the energy of the PL peak. The x-axis is not in scale, for image clarity.

emission energy of up to 40 meV, corresponding to a doping of $\sim 2 \times 10^{18}$ cm^{-3} as confirmed by APT. p-Doping does not affect the peak energy, so that the emission peak is always centered at ~1.42 eV, hinting that the carrier concentration in n-doped samples is much higher than in p-doped samples. Zn is known to be more difficult to incorporate if the growth temperature is raised over ≈700°C [39, 40]; recent results published in literature also support this conclusion [41, 42]. This inference is further confirmed by measurements performed with APT of nanowires identical to those presented here: at the highest Zn molar fraction (7.4×10^{-6}), the Zn concentration is $<10^{17}$ cm^{-3}, which is difficult to discern from the ppm noise level of the instrument (1 ppm is 4×10^{16} cm^{-3} in InP). At lower molar fractions, thus, the dopant concentration cannot be estimated.

p- and n-doping influences the total intensity of PL, in opposite ways: increasing Si doping leads to a decrease in emission strength (about a factor 3), while augmenting the DEZn molar flow appears to be beneficial, leading to a 10-fold increase in PL intensity (Figure 5). It is interesting to note that the PL intensity of p-doped nanowires is always much smaller than that of n-doped though (between factors of 3 and 1000, depending on the values used to compare). Furthermore, increasing the dopant molar fraction results in a shorter minority recombination lifetime in both cases, as shown in Figure 5(b).

Two key equations must be introduced in order to explain this phenomenon. First, it must be considered that, under any kind of excitation, the radiative recombination rate is defined as

$$R_{\text{ext}} \propto (n_0 + \Delta n)(p_0 + \Delta p), \tag{7}$$

in which R_{ext} is the radiative recombination rate, n_0 (p_0) are the equilibrium concentrations of electrons (holes), and Δn (Δp) are the density of excited carriers (in this case, photoexcited). In particular, it is important to note how, following this equation, an increase in the doping atom concentration (n_0 or p_0) should result in an increase in R_{ext}, which results in a decrease in minority carrier recombination lifetime. An increase in the recombination rate would then correspond to an increase in the PL intensity (when normalized to the integration time) and thus in an increase in the $\eta_{\text{ext}}^{\text{PL}}$, which, if the P_{esc} is constant, means that the $\eta_{\text{int}}^{\text{PL}}$ is enhanced. The contribution of nonradiative recombination must also be taken into account though, as expressed by the relation

$$\eta_{\text{int}}^{\text{PL}} = \frac{\tau_{\text{r}}^{-1}}{\tau_{\text{r}}^{-1} + \tau_{\text{nrad}}^{-1}}, \tag{8}$$

where τ_{r}^{-1} is directly related to the radiative recombination rate R_{ext} just introduced [8, 44].

It is thus clear that two mechanisms take place when the dopant concentration is increased: as the equilibrium carrier concentration is larger, leading to an increase in the R_{ext}, the τ_{nrad}^{-1} is also increased at the same time, as the number of impurity-related nonradiative recombination centers is increased. The different behaviors of undoped and p- and n-doped nanowires are then explained by comparing their dependence on carrier concentration of the PL intensity ($\propto \eta_{\text{int}}^{\text{PL}}$) and the minority carrier recombination lifetime ($\propto R_{\text{ext}}$) (Figure 5):

(i) n-Doped NW: at the lowest DTBSi molar fraction considered, the dopant atom concentration is already relatively high ($\approx 8 - 10 \times 10^{16}$ cm^{-3}), so that as the dopant concentration is increased, the contribution to $\eta_{\text{int}}^{\text{PL}}$ of nonradiative recombination is rising more quickly than the radiative recombination is, as is expected in this doping range: the PL intensity is thus lowered [32]. This is further proved by the fact that with increasing carrier concentration (assumed to be linearly dependent on the dopant molar fraction), the radiative recombination rate does not increase linearly, but appears to saturate very quickly (Figures 5(b) and 5(c)). The saturation in the recombination rate is then attributed to the increased contribution from nonradiative recombination; as the PL intensity is nevertheless larger than in the p -doped case, it would be explained by a nonradiative recombination rate lower on absolute terms

(ii) p-Doped NW: the introduction of Zn increases the recombination rate as p_0 is increased (as in equation (7)), and consequently the radiative lifetime is reduced. The PL intensity increase with higher DEZn is explained by the fact that since the doping is still rather low ($<10^{17}$ cm^{-3}), the dominant variation in $\eta_{\text{int}}^{\text{PL}}$ would be the increased τ_{r}^{-1}. In comparison to the undoped case, however, with a small amount of Zn atoms, the τ_{nrad}^{-1} is suggested to be much higher, as the PL intensity is much lower (cf. equation (8)). Raising the DEZn molar fraction and thus the dopant atom concentration, which is the concentration of impurities, does not appear to augment τ_{nrad}^{-1} further in a substantial manner instead. In the range available, in fact, if a similar

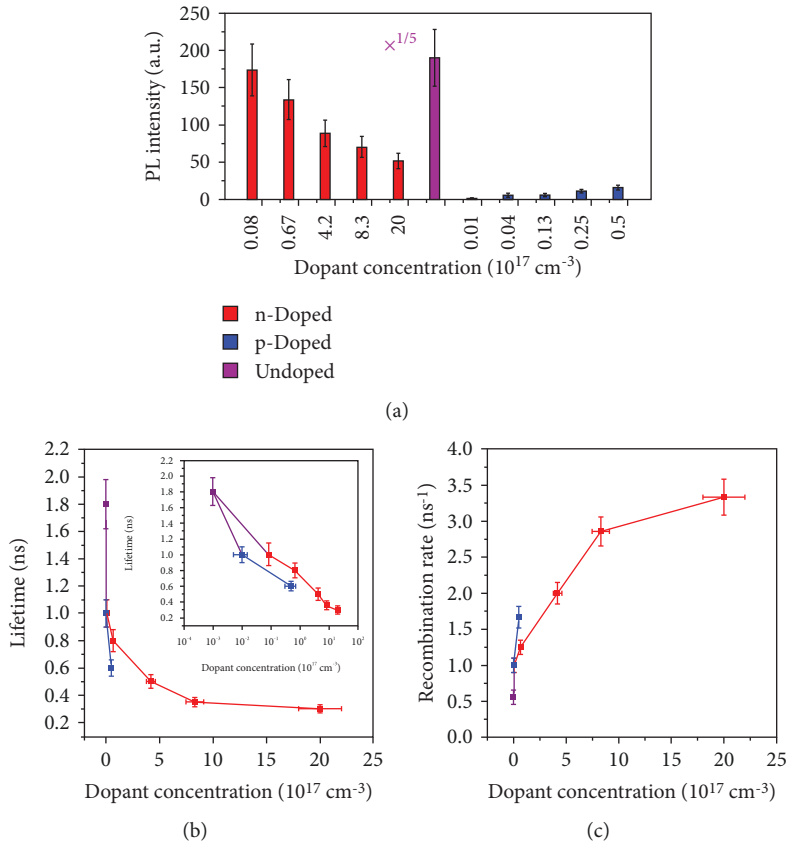

FIGURE 5: Effect on optical properties as a function of dopant atom concentration, extracted by APT measurements on highly doped samples, for undoped (purple) as well as p (red) and n (blue) doping. (a) Integrated PL intensity dependent on the dopant atom concentration, measured at a laser intensity of ~1000 W/cm^2. The x-axis is not in scale, for image clarity. (b) Minority carrier recombination lifetime. p-Doped samples have shorter lifetime at comparable dopant concentrations. The inset shows the same data, with the x-axis in logarithmic scale to further prove the difference between p- and n-doped samples. (c) Recombination rate, calculated as the inverse of the lifetime, showing once again the faster recombination rate exhibited by p-doped nanowires. In (b) and (c), the purple dot represents the lifetime (rate) of an undoped sample grown in identical conditions, without introducing dopants. For this sample, a background intrinsic dopant concentration of 10^{15} cm^{-3} is considered, in accordance to typical values of intrinsic carrier concentration for MOCVD-grown InP [43].

doping atom concentration is considered, p-doped NW have a lower lifetime and a correspondent higher recombination rate than n-doped NW (Figures 5(b) and 5(c)), so no saturation is observed, in contrast with the n-doped case. Several publications have already demonstrated how the internal radiative efficiency of p-doped InP is much lower than n-doped: this is often attributed to a large density of deep trap levels related to Zn-induced neutral acceptor centers, which result in nonradiative recombination dominance [45, 46]. The PL intensity has an ambiguous behavior though, as it is very high for undoped NW, is heavily reduced for the lowest DEZn molar fraction, and increases slightly again as DEZn becomes larger. A possible explanation is that since the molar fraction of DEZn is rather high (comparable or even larger than the TMI), it is densely present in the chamber. Even if it is not incorporated in the bulk of the nanowires, it can still accumulate at the surface of the nanowire lateral facets, where it would heavily increase the surface recombination. A possible explanation for the different incorporation of Zn on the top surface (where the axial growth takes place) and the lateral facets (where no radial growth is observed) is explained by the fact that lateral facets have different crystalline orientations, which result in a dissimilar Zn atom adsorption [28]. The adsorption is not influenced by an increased DEZn molar fraction, as even at the lowest flow there would be an excess of Zn atoms. Zn is often deemed responsible for stimulating point defect constitution, for example, following the introduction of interstitial Zn or a phosphorus divacancy linked to Zn ($V_P - Zn_i - V_P$) [47]. The incorporation in the core part of the nanowires is instead dependent on the molar fraction, resulting in the strange behavior of PL intensity. Atoms present at the surface are difficult to measure by APT or other techniques though, so it is difficult to prove unequivocally that Zn deposited at the surface is responsible for this phenomenon

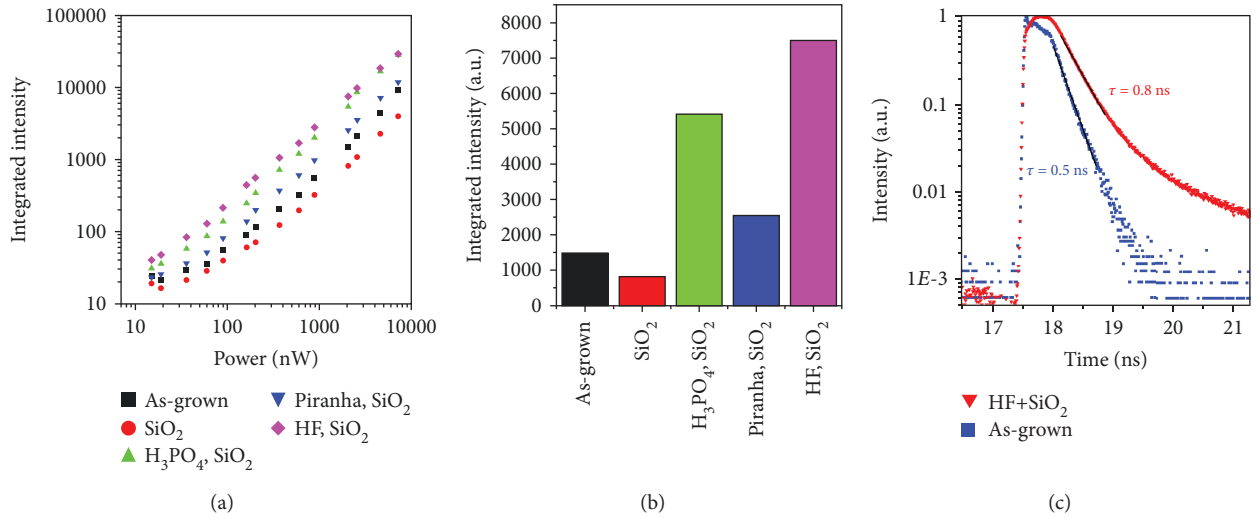

FIGURE 6: Effect of device fabrication on nanowire PL intensity. (a) PL intensity as a function of incident laser intensity, plotted with different lines representing different cleaning and passivation stages. The highest PL signal is obtained by cleaning nanowires in a 1% diluted HF solution and capping them with SiO_2. (b) Integrated PL intensity measured at a laser power of 75 W/cm^2, showing the same data in panel (a). (c) Time-resolved photoluminescence of the same as-grown and HF + SiO_2 samples, measured at a laser intensity of 1.4 W/cm^2.

(iii) Undoped NW: the radiative lifetime is relatively long (~1.8 ns) compared to doped nanowires, so the recombination rate must be small. Nevertheless, since the PL and thus the internal radiative efficiency are high, the nonradiative recombination rate must be very low. It is reasonable, since no intentional impurities are introduced, so the imperfection and trap density should be small. Surface recombination can be expected to be the major source of nonradiative recombination

In the case of bulk InP, the reported minority carrier radiative recombination lifetime (a few tens of ns) is much longer than for nanowires discussed in the previous section though (~1 ns): surface recombination is undoubtedly responsible for a large part of this decrease, so an adequate passivation design should be implemented in nanowires to improve their performance. Atomic layer deposition (ALD) of $PO_x + Al_2O_3$ thin layers, deposited on the same undoped nanowires previously mentioned, has been demonstrated to greatly increase radiative lifetime. A 3-fold enhancement of radiative lifetime (up to >5 ns) is achieved, which results in a $\eta_{\text{ext}}^{\text{PL}}$ enhancement of more than an order of magnitude, since τ_{rad} is increased at the same time as $\tau_{n\text{rad}}$ is decreased [48].

3.4. Effect of Device Processing. As the intended solar cell application of the nanowires presented in this study requires several processing steps, it is important to study the effect of device fabrication on the nanowire PL. The procedure, discussed previously in detail [18], starts with a cleaning and passivation step and continues with nanowire array planarization and front-side contacting.

Nanowires possess a rather high surface-to-volume ratio, which is around 5 times larger than the surface of a bulk layer if cylindrical NW are considered, with 2 μm length, 500 nm pitch, and 180 nm diameter. Surface protection and passivation is thus crucial: in the case of VLS InP nanowires, it has been demonstrated that during growth the surface easily incorporates defects, which cannot be removed by the in situ HCl etching. These imperfections are eliminated by removing the outer part of the nanowires with a short postgrowth *ex situ* Piranha etch (25 s in $H_2SO_4 : H_2O_2 : H_2O$ 3 : 1 : 1), which allows improving the efficiency of the device from ~1% up to 11.1% [18, 19]. For selective area nanowires, both a dielectric coating and a lattice-mismatched window layer have been proposed as performance-enhancing passivations [14, 41], together with ALD deposition, which as previously said have been demonstrated to substantially increase the nanowire optical properties [48].

In Figures 6(a) and 6(b), several different cleaning solutions are thus evaluated by measuring the integrated intensity of PL emission of intrinsic nanowires. SiO_2 deposited by PECVD at 300°C is used as passivation, as it has been demonstrated to be effective in several instances both for InP and for other III – V materials [15, 16, 18, 49]. The use of SiO_2 only, without any cleaning beforehand, appears to be detrimental compared to the as-grown sample, most likely because without any cleaning the native oxide formed on the nanowire sidewalls prevents any effective passivation of the material. Three cleaning solutions, all in combination with SiO_2 deposition after the cleaning, are then considered: Piranha, diluted (10%) phosphoric acid, and diluted (1%) HF etching. Piranha appears to improve slightly the performance relative to as-grown nanowires, but is not as effective as oxide-only removing agents like H_3PO_4 or HF. In fact, Piranha removes also InP, so that the effective nanowire volume is decreased, lowering the absorption: the decrease in absorptance does not justify the reduction of PL intensity of a factor of ~2, though, so it is possible that the nanowire sidewalls are damaged as a result.

H_3PO_4 and HF instead, in combination with SiO_2 deposition, both increase significantly the PL intensity: this is attributed to the gentle oxide etch performed by both solutions. HF yields a slightly better performance as a result of the different chemistry of the postcleaning surface. In fact, H_3PO_4 cleaning results in a hydrophobic surface which is terminated by hydrogen atoms bound to phosphorous sites, while HF produces a hydrophilic fluorine-terminated surface on the indium sites [50]. When heated during the SiO_2 deposition under N_2 atmosphere, the F-termination is removed quickly, so that SiO_2 would be deposited directly on the nanowires. The H atoms resulting from H_3PO_4, instead, are not removed and thus alter the surface of the nanowires and the interface with the deposited SiO_2 [50]. Additionally, a significant improvement has also been demonstrated by HF passivation in single-nanowire solar cells [16]. Dielectric coating is also expected to increase the absorptance of the nanowires, but it cannot explain a ~3 – fold increase in PL intensity, which is thus attributed to the beneficial passivation. A further demonstration of the enhanced performance is in Figure 6(c), where time-resolved photoluminescence of p – n nanowires grown at 730°C with a V/III ratio of 114 is compared between an as-grown sample and one with the best passivation scheme HF + SiO_2. A clear improvement in the minority carrier radiative recombination lifetime is observed, from 0.5 ns to 0.8 ns, which suggests a reduction of surface recombination thanks to the passivation. The shorter lifetime compared with the intrinsic case presented in the previous section is caused by the doping (molar fractions are 4×10^{-8} for DTBSi, 7.4×10^{-5} for DEZn), which as discussed previously decreases the minority carrier recombination lifetime. p – n nanowires have also been tested at all further stages of device fabrication: no significant effect on the PL intensity is observed at different steps. This is expected since no further material passivation is performed, and all processing is performed at low temperature, so that the nanowires are not affected by it. The variation between samples is in the order of ±10%, which is the same range of deviation as between different identical samples and regions of the same sample.

4. Conclusion

The internal radiative efficiency of the nanowires is studied and optimized by varying growth conditions, such as the temperature and the doping molar flows. It is found that the ideal parameters are a temperature of 730°C and a V/III ratio of 114, while a complex influence of dopants is determined. Both dopants result in a decrease in the minority carrier recombination lifetime and a reduction in the PL intensity compared to undoped nanowires. In particular, the introduction of Zn, the p-dopant, results in a strong decrease in the PL intensity of the nanowires, caused by the inclusion of nonradiative recombination centers. Furthermore, by investigating the effect of device fabrication steps, it is found that with a cleaning and passivation procedure based on diluted HF and SiO_2 deposition, the nanowire optical properties are improved.

Data Availability

The photoluminescence data used to support the findings of this study are available from the corresponding author A. Cavalli upon request (at a.cavalli.phd@gmail.com).

Conflicts of Interest

The authors declare no conflicts of interest.

Authors' Contributions

A.C. conceived and designed the experiment, as well as fabricated and measured the samples, and wrote the manuscript. J.E.M.H. and E.P.A.M.B. provided the theoretical background to the study and the result interpretation, as well as supervised the study and strongly supported and encouraged its development. All authors reviewed, discussed, and approved the results and conclusions of this article.

Acknowledgments

The Dutch Technology Foundation STW (Project 11826), which is part of the Netherlands Organization for Scientific Research (NWO), and which is partly funded by the Ministry of Economic Affairs, The Netherlands, supports this research. We would like to acknowledge Rene Van Veldhoven for the exceptional work and care for the MOVPE systems, Dick van Dam and Yingchao Cui for the outstanding contribution to discussions, Marcel Verheijen for the TEM measurements, and the technical support from the NanoLab@TU/e cleanroom.

References

[1] P. Prete, *Nanowires*, 2010, Intech.

[2] A. Cavalli, A. Dijkstra, J. E. M. Haverkort, and E. P. A. M. Bakkers, "Nanowire polymer transfer for enhanced solar cell performance and lower cost," *Nano-Structures & Nano-Objects*, vol. 16, pp. 59–62, 2018.

[3] N. Anttu, A. Abrand, D. Asoli et al., "Absorption of light in InP nanowire arrays," *Nano Research*, vol. 7, no. 6, pp. 816–823, 2014.

[4] D. van Dam, N. J. J. van Hoof, Y. Cui et al., "High-efficiency nanowire solar cells with omnidirectionally enhanced absorption due to self-aligned indium–tin–oxide Mie scatterers," *ACS Nano*, vol. 10, no. 12, pp. 11414–11419, 2016.

[5] B. Ganjipour, A. W. Dey, B. M. Borg et al., "High current density Esaki tunnel diodes based on GaSb-InAsSb heterostructure nanowires," *Nano Letters*, vol. 11, no. 10, pp. 4222–4226, 2011.

[6] E. C. Garnett, M. L. Brongersma, Y. Cui, and M. D. McGehee, "Nanowire solar cells," *Annual Review of Materials Research*, vol. 41, no. 1, pp. 269–295, 2011.

[7] L. Gao, Y. Cui, J. Wang et al., "Photoelectrochemical hydrogen production on InP nanowire arrays with molybdenum sulfide electrocatalysts," *Nano Letters*, vol. 14, no. 7, pp. 3715–3719, 2014.

[8] J. E. M. Haverkort, E. C. Garnett, and E. P. A. M. Bakkers, "Fundamentals of the nanowire solar cell: optimization of the

open circuit voltage," *Applied Physics Reviews*, vol. 5, no. 3, article 031106, 2018.

[9] R. S. Wagner and W. C. Ellis, "Vapor-liquid-solid mechanism of single crystal growth," *Applied Physics Letters*, vol. 4, no. 5, pp. 89-90, 1964.

[10] J. Wang, S. R. Plissard, M. A. Verheijen, L. F. Feiner, A. Cavalli, and E. P. A. M. Bakkers, "Reversible switching of InP nanowire growth direction by catalyst engineering," *Nano Letters*, vol. 13, no. 8, pp. 3802–3806, 2013.

[11] A. Cavalli, J. Wang, I. E. Zadeh et al., "High-yield growth and characterization of <100>InP p-n diode nanowires," *Nano Letters*, vol. 16, no. 5, pp. 3071–3077, 2016.

[12] Q. Gao, D. Saxena, F. Wang et al., "Selective-area epitaxy of pure wurtzite InP nanowires: high quantum efficiency and room-temperature lasing," *Nano Letters*, vol. 14, no. 9, pp. 5206–5211, 2014.

[13] K. Tomioka, M. Yoshimura, and T. Fukui, "A III-V nanowire channel on silicon for high-performance vertical transistors," *Nature*, vol. 488, no. 7410, pp. 189–192, 2012.

[14] M. Yoshimura, E. Nakai, K. Tomioka, and T. Fukui, "Indium phosphide core-shell nanowire array solar cells with lattice-mismatched window layer," *Applied Physics Express*, vol. 6, no. 5, article 52301, 2013.

[15] S. A. Mann, S. Z. Oener, A. Cavalli, J. E. M. Haverkort, E. P. A. M. Bakkers, and E. C. Garnett, "Quantifying losses and thermodynamic limits in nanophotonic solar cells," *Nature Nanotechnology*, vol. 11, no. 12, pp. 1071–1075, 2016.

[16] S. Z. Oener, A. Cavalli, H. Sun, J. E. M. Haverkort, E. P. A. M. Bakkers, and E. C. Garnett, "Charge carrier-selective contacts for nanowire solar cells," *Nature Communications*, vol. 9, no. 1, article 3248, 2018.

[17] T. Mårtensson, P. Carlberg, M. Borgström, L. Montelius, W. Seifert, and L. Samuelson, "Nanowire arrays defined by nanoimprint lithography," *Nano Letters*, vol. 4, no. 4, pp. 699–702, 2004.

[18] Y. Cui, J. Wang, S. R. Plissard et al., "Efficiency enhancement of InP nanowire solar cells by surface cleaning," *Nano Letters*, vol. 13, no. 9, pp. 4113–4117, 2013.

[19] A. Cavalli, Y. Cui, S. Kölling et al., "Influence of growth conditions on the performance of InP nanowire solar cells," *Nanotechnology*, vol. 27, no. 45, article 454003, 2016.

[20] T. T. T. Vu, *Nanowire Photoluminescence for Photovoltaics*, Phd thesis, 2015.

[21] S. Koelling, A. Li, A. Cavalli et al., "Atom-by-atom analysis of semiconductor nanowires with parts per million sensitivity," *Nano Letters*, vol. 17, no. 2, pp. 599–605, 2017.

[22] Y. Kitauchi, Y. Kobayashi, K. Tomioka et al., "Structural transition in indium phosphide nanowires," *Nano Letters*, vol. 10, no. 5, pp. 1699–1703, 2010.

[23] S. Assali, I. Zardo, S. Plissard et al., "Direct band gap wurtzite gallium phosphide nanowires," *Nano Letters*, vol. 13, no. 4, pp. 1559–1563, 2013.

[24] T. T. T. Vu, T. Zehender, M. A. Verheijen et al., "High optical quality single crystal phase wurtzite and zincblende InP nanowires," *Nanotechnology*, vol. 24, no. 11, article 115705, 2013.

[25] S. Paiman, Q. Gao, H. H. Tan et al., "The effect of V/III ratio and catalyst particle size on the crystal structure and optical properties of InP nanowires," *Nanotechnology*, vol. 20, no. 22, article 225606, 2009.

[26] Y. Cui, D. van Dam, S. A. Mann et al., "Boosting solar cell photovoltage via nanophotonic engineering," *Nano Letters*, vol. 16, no. 10, pp. 6467–6471, 2016.

[27] H. J. Joyce, Q. Gao, H. H. Tan et al., "Unexpected benefits of rapid growth rate for III-V nanowires," *Nano Letters*, vol. 9, no. 2, pp. 695–701, 2009.

[28] M. Kato, T. Akiyama, K. Nakamura, and T. Ito, "Effects of Zn doping on the surface structure and initial growth processes of InP thin film layers on InP(111)B substrate," *e-Journal of Surface Science and Nanotechnology*, vol. 13, no. 0, pp. 147–150, 2015.

[29] K. L. Fry, C. P. Kuo, C. A. Larsen, R. M. Cohen, G. B. Stringfellow, and A. Melas, "OMVPE growth of InP and Ga0.47ln0.53as using ethyldimethylindium," *Journal of Electronic Materials*, vol. 15, no. 2, pp. 91–96, 1986.

[30] K. Ikejiri, Y. Kitauchi, K. Tomioka, J. Motohisa, and T. Fukui, "Zinc blende and wurtzite crystal phase mixing and transition in indium phosphide nanowires," *Nano Letters*, vol. 11, no. 10, pp. 4314–4318, 2011.

[31] H. Q. Zheng, K. Radahakrishnan, S. F. Yoon, and G. I. Ng, "Electrical and optical properties of Si-doped InP grown by solid source molecular beam epitaxy using a valved phosphorus cracker cell," *Journal of Applied Physics*, vol. 87, no. 11, article 7988, 7993 pages, 2000.

[32] M. Wanlass, "Systems and methods for advanced ultra-high-performance InP solar cells," Patent US20150280042, 2015.

[33] G. S. Pomrenke, "Evidence of amphoteric behavior of Si in VPE InP," *Journal of Crystal Growth*, vol. 64, no. 1, pp. 158–164, 1983.

[34] S. Leu, H. Protzmann, F. Höhnsdorf, W. Stolz, J. Steinkirchner, and E. Hufgard, "Si-doping of MOVPE grown InP and GaAs by using the liquid Si source ditertiarybutyl silane," *Journal of Crystal Growth*, vol. 195, no. 1-4, pp. 91–97, 1998.

[35] L. Diehl, D. Bour, S. Corzine et al., "High-power quantum cascade lasers grown by low-pressure metal organic vapor-phase epitaxy operating in continuous wave above 400K," *Applied Physics Letters*, vol. 88, no. 20, article 201115, 2006.

[36] M. Bugajski and W. Lewandowski, "Concentration-dependent absorption and photoluminescence of *n*-type InP," *Journal of Applied Physics*, vol. 57, no. 2, pp. 521–530, 1985.

[37] S. Arab, M. Yao, C. Zhou, P. Daniel Dapkus, and S. B. Cronin, "Doping concentration dependence of the photoluminescence spectra of n-type GaAs nanowires," *Applied Physics Letters*, vol. 108, no. 18, article 182106, 2016.

[38] M. T. Borgström, E. Norberg, P. Wickert et al., "Precursor evaluation for *in situ* InP nanowire doping," *Nanotechnology*, vol. 19, no. 44, article 445602, 2008.

[39] W. T. Tsang, F. S. Choa, and N. T. Ha, "Zinc-doping of InP during chemical beam epitaxy using diethylzinc," *Journal of Electronic Materials*, vol. 20, no. 8, pp. 541–544, 1991.

[40] F. G. Kellert, S. R. Sloan, M. J. Ludowise, and J. E. Turner, "Zn-doping in OMVPE grown lnP:Zn/lnGaAs/lnP*p-i-n* double heterojunctlons with lnGaAs:Zn contacting layers," *Journal of Electronic Materials*, vol. 21, no. 10, pp. 983–987, 1992.

[41] Z. Zhong, Z. Li, Q. Gao et al., "Efficiency enhancement of axial junction InP single nanowire solar cells by dielectric coating," *Nano Energy*, vol. 28, pp. 106–114, 2016.

[42] T. Haggren, G. Otnes, R. Mourão et al., "InP nanowire p-type doping via zinc indiffusion," *Journal of Crystal Growth*, vol. 451, pp. 18–26, 2016.

[43] J. A. Long, V. G. Riggs, and W. D. Johnston Jr, "Growth of Fe-doped semi-insulating InP by MOCVD," *Journal of Crystal Growth*, vol. 69, no. 1, pp. 10–14, 1984.

[44] U. Rau, U. W. Paetzold, and T. Kirchartz, "Thermodynamics of light management in photovoltaic devices," *Physical Review B*, vol. 90, no. 3, article 35211, 2014.

[45] Y. Rosenwaks, Y. Shapira, and D. Huppert, "Picosecond time-resolved luminescence studies of surface and bulk recombination processes in InP," *Physical Review B*, vol. 45, no. 16, pp. 9108–9119, 1992.

[46] Y. Rosenwaks, I. Tsimberova, H. Gero, and M. Molotskii, "Minority-carrier recombination in p – InP single crystals," *Physical Review B*, vol. 68, no. 11, article 115210, 2003.

[47] A. J. Howard, B. Pathangey, Y. Hayakawa, T. J. Anderson, C. Blaauw, and A. J. SpringThorpe, "Application of the point-defect analysis technique to zinc doping of MOCVD indium phosphide," *Semiconductor Science and Technology*, vol. 18, no. 8, pp. 723–728, 2003.

[48] L. E. Black, A. Cavalli, M. A. Verheijen, J. E. M. Haverkort, E. P. A. M. Bakkers, and W. M. M. Kessels, "Effective surface passivation of InP nanowires by atomic-layer-deposited Al_2O_3 with PO_x interlayer," *Nano Letters*, vol. 17, no. 10, pp. 6287–6294, 2017.

[49] S. A. Chevtchenko, M. A. Reshchikov, Q. Fan et al., "Study of SiN_x and SiO_2 passivation of GaN surfaces," *Journal of Applied Physics*, vol. 101, no. 11, article 113709, 2007.

[50] Y. Sun, Z. Liu, F. Machuca, P. Pianetta, and W. E. Spicer, "Optimized cleaning method for producing device quality InP(100) surfaces," *Journal of Applied Physics*, vol. 97, no. 12, article 124902, 2005.